



Structure evolution of as-cast metastable Fe-38Ga alloy towards equilibrium



T.N. Vershinina^{a,b,*}, I.A. Bobrikov^{a,c}, S.V. Sumnikov^{a,c}, A.M. Balagurov^{a,c,d}, A.K. Mohamed^{c,e}, I.S. Golovin^{c,e}

^a Joint Institute for Nuclear Research, Joliot-Curie 6, 141980 Dubna, Russian Federation

^b Dubna State University, Universitetskaya 19, 141980 Dubna, Russian Federation

^c National University of Science and Technology "MISIS", Leninskiy ave. 4, 119991 Moscow, Russian Federation

^d Lomonosov Moscow State University, GSP-1, Leninskie Gory, 119991 Moscow, Russian Federation

^e Moscow Polytechnic University, B. Semenovskay 38, 107023 Moscow, Russian Federation

ARTICLE INFO

Article history:

Received 29 July 2021

Received in revised form 26 August 2021

Accepted 28 August 2021

Available online 30 August 2021

Keywords:

Fe-Ga alloys

Phase transformation

Neutron diffraction

ABSTRACT

The evolution of the structural phases of the Fe-38.4 at%Ga alloy was studied in neutron diffraction experiments performed with high-intensity continuous scanning in a wide temperature range. The as-cast alloy consists of ~70% Fe₁₃Ga₉ intermetallic and ~30% bcc-based disordered A2 solid solution (or its partially ordered/short-range ordered B2 variant). The research proves that during the first heating of the cast alloy, the Fe₁₃Ga₉ phase is stable up to T ≈ 550 °C, then it transforms into α-Fe₆Ga₅, fcc-based L1₂ and B2 phases. At the same temperature, the disorder-order transition A2 → B2 begins, ending at T ≈ 720 °C. The Fe₁₃Ga₉ phase does not restore during subsequent cooling and next heating and cooling cycles. The structural parameters of the identified phases are refined. The research also shows that the transition temperatures depend on the alloy prehistory.

© 2021 Elsevier B.V. All rights reserved.

1. Introduction

Fe-Ga-based alloys are widely recognized as materials with special functional magnetic properties that lead to the formation of several interesting physical effects. A surge of interest in Fe-xGa alloys occurred in the early 2000s after discovering increased values of the magnetostriction constant, which for the region $x \approx 18\text{--}28\text{ at\%}$ is 10–20 times higher than for iron [1]. As a result, the structural features of the Fe-xGa compositions in the range of the phase diagram up to $x \approx 30\text{ at\%}$ are well studied and widely presented in the literature [2–4]. On the contrary, the region of high gallium concentrations ($x > 33\text{ at\%}$) has not yet been studied in sufficient depth. In particular, there is still no complete understanding of what phases can form under certain conditions, and their atomic structure continues to be refined. For example, for Fe-38.4Ga and Fe-45Ga, their

phase composition after quenching from the melt and structural characteristics at room temperature were determined only recently [5,6]. It was also shown that a two-phase nonequilibrium state is formed upon Fe-38.4Ga quenching. One of the detected phases is a disordered bcc A2 phase or a partially ordered B2 phase with a low level of order, and the second phase, as shown by diffraction methods, belongs to the intermetallic Ni₁₃Ga₉ structural type (space group C2/m). Previously, the existence of this phase was only mentioned in Ref. [7] as an M-phase and as Fe₁₃Ga₉ at Ref. [8], but information about the atomic structure was not presented. A detailed analysis of neutron and X-ray diffraction patterns and the use of numerical simulation methods allowed the authors of Ref. [5] to establish the cell parameters and the atomic coordinates of the Fe₁₃Ga₉ phase.

In this paper, the stability of the Fe₁₃Ga₉ phase under heating conditions and the features of phase transitions in the nonequilibrium state of the Fe-38.4Ga alloy are studied. The analysis of the evolution of the phase composition of the alloy in the framework of two cycles of its heating and subsequent cooling is also carried out. *In situ* real-time neutron diffraction was used as the main experimental method. The high neutron penetration depth allows observation of bulk effects and exclusion of the influence of the surface layer (evaporation of gallium) and local inhomogeneities of

* Correspondence to: Joint Institute for Nuclear Research, 6 Joliot-Curie St, Dubna, Russian Federation.

E-mail addresses: vershinina@nf.jinr.ru (T.N. Vershinina), bobrikov@nf.jinr.ru (I.A. Bobrikov), sumnikovsv@gmail.com (S.V. Sumnikov), bala@nf.jinr.ru (A.M. Balagurov), abdelkarim.abdelkarim@feng.bu.edu.eg (A.K. Mohamed), i.golovin@mis.ru (I.S. Golovin).

the structure. It also allows interpretation of the differential scanning calorimetry, dilatometry, and internal friction data.

2. Experimental methods

2.1. Material

Fe-Ga alloy with nominal compositions 38 at% Ga was produced by induction melting (Indutherm MC-20 V mini furnace) from pure Fe (commercial purity) and pure Ga (99.99%) in a ceramic crucible under protective high-purity argon gas and cast into a copper mold of the inner dimension of $4 \times 16 \times 60 \text{ mm}^3$. The chemical composition analysis by EDX Spectroscopy revealed that the composition is indeed Fe-(38.4 \pm 0.1) at% Ga. The EDX was calibrated based on high purity Fe and Ga. This calibration process gives the tolerance of (\pm 0.1). The standard error of measurement of the chemical composition is 0.1–0.2%. In this paper, we use only atomic % to indicate chemical composition.

2.2. Neutron diffraction experiments

Neutron diffraction patterns (NDPs) were measured at a high-resolution ($\Delta d/d \approx 0.0015$) Fourier diffractometer (HRFD) operating at the IBR-2 pulsed reactor in JINR (Dubna, Russia) [9]. This is a time-of-flight (TOF) instrument that can be easily switched between high resolution ($\Delta d/d \approx 0.0015$) and high-intensity ($\Delta d/d \approx 0.015$) diffraction modes, which are both used for the analysis of phase transformations in Fe-Ga alloys.

In a high-resolution mode, the diffraction patterns were measured for initial (as-cast) and final (after two cycles of heating-cooling) states in the range $d_{hkl} = 0.5\text{--}5 \text{ \AA}$. The data evaluation by the Rietveld method was carried out on the data corresponding to a d -spacing range of 0.8–3.6 \AA using the software package FullProf [10].

In situ study, which includes two cycles of heating up to 900 $^{\circ}\text{C}$ and the following cooling to room temperature, were performed in the high-intensity mode. The holding time at the final heating temperature was 20 min in the first cycle and 40 min in the second cycle. The *in situ* experiment was carried out with heating and cooling rates close to 2 $^{\circ}\text{C}/\text{min}$. The diffraction patterns were measured continuously with a 2 min exposure time in a d -spacing range of 0.8–5 \AA . The data evaluation by the Rietveld method was carried out on the data corresponding to a d -spacing range of 0.8–3.6 \AA using the software package MAUD [11].

2.3. Calorimetry and dilatometry

The Labsys Setaram system was used to perform Conventional differential scanning calorimetry (DSC) measurements with a heating up to 900 $^{\circ}\text{C}$ and a heating rate of 10 $^{\circ}\text{C}/\text{min}$ in an air atmosphere to characterize the intervals of the alloys' phase transitions. The dilatometry (DT) tests were recorded at temperatures ranging from 20 $^{\circ}\text{C}$ to 800 $^{\circ}\text{C}$ at a heating rate of 5 $^{\circ}\text{C}/\text{min}$ using a Dilatometer Linseis L75.

2.4. Temperature dependent internal friction tests

The temperature-dependent internal friction (TDIF) tests performed on the same alloy with a heating rate of 2 $^{\circ}\text{C}/\text{min}$ in an air atmosphere using bending forced vibrations at DMA Q800 TA Instruments up to 600 $^{\circ}\text{C}$ were recently published in Ref. [12] and are also used in this paper for discussions.

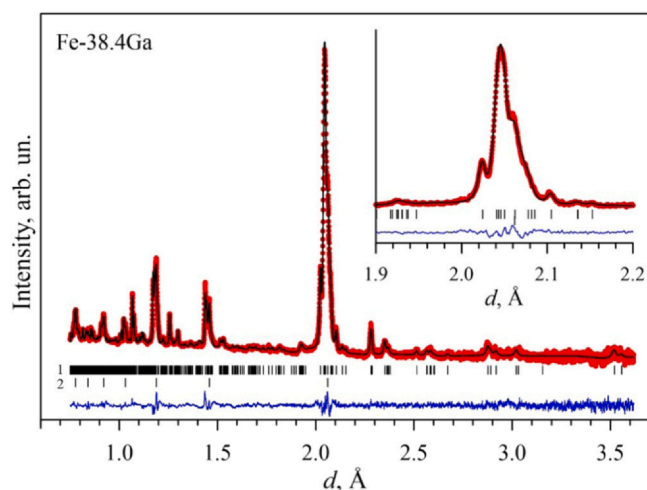


Fig. 1. ND pattern (high resolution) of the Fe-38.4Ga as-cast sample processed by the Rietveld method. The experimental points and the calculated line are shown. The vertical bars indicate the peak positions of $\text{Fe}_{13}\text{Ga}_9$ (1) and A2 (2).

3. Results

3.1. Neutron diffraction

The phase analysis conducted using neutron diffraction (Fig. 1) showed that in the initial as-cast state, the Fe-38.4Ga alloy contains $\text{Fe}_{13}\text{Ga}_9$ (sp.gr. $C2/m$) and A2 (sp.gr. $Im\bar{3}m$) (or partially ordered B2 (sp.gr. $Pm\bar{3}m$)) phases in the amount of $\sim 70\%$ and $\sim 30\%$, respectively. The superstructure diffraction lines of the B2 phase (100 and others) have weak intensities, and they can be skipped in the pattern in the case of a small phase content or low ordering level. This is why we will further denote the bcc-based state without a clear presence of the B2 superstructure lines as A2/B2. The $\text{Fe}_{13}\text{Ga}_9$ phase was previously detected in the studied alloy, and the results of its crystal structure analysis are given in the paper [5].

The *in situ* NDPs measured under heating and subsequent cooling of the as-cast sample with a rate of 2 $^{\circ}\text{C}/\text{min}$ are shown in Fig. 2, and typical diffraction patterns measured during heating at several particular temperatures are presented in Fig. 3.

The Rietveld method was used to estimate the volume fractions of the coexisting phases and their evolution upon heating. It follows from Fig. 4 that the A2/B2 + $\text{Fe}_{13}\text{Ga}_9$ state is stable up to $T \approx 550 \text{ }^{\circ}\text{C}$. Then the metastable $\text{Fe}_{13}\text{Ga}_9$ phase disappears, and two equilibrium phases, fcc-based $L1_2$ (sp.gr. $Pm\bar{3}m$) and monoclinic $\alpha\text{-Fe}_6\text{Ga}_5$ (sp.gr. $C2/m$), appear in addition to A2/B2.

The volume occupied by the A2/B2 phases and the ordering level begin to increase markedly at $T > 550 \text{ }^{\circ}\text{C}$, and the superstructure peak 100 becomes clearly visible already at $T \approx 600 \text{ }^{\circ}\text{C}$ (Fig. 3b). With a further increase in temperature, $L1_2$ completely disappears at $T \approx 660 \text{ }^{\circ}\text{C}$, and then $\alpha\text{-Fe}_6\text{Ga}_5$ also disappears at $T \approx 720 \text{ }^{\circ}\text{C}$. Only the B2 phase is observed in a temperature range of above 720 $^{\circ}\text{C}$. Contrary to the expectation [13], there is a noticeable increase in the unit cell parameter of the A2/B2 phase from 2.92 to 2.94 \AA at $T \approx 570 \text{ }^{\circ}\text{C}$ (Fig. 5), which is also visible in Fig. 2. The possible cause of this effect is discussed in the next section. It should be noted that the indicated transition temperatures are determined from the actual appearance or disappearance of diffraction peaks of the corresponding phases with a continuous temperature change, and the real region of their existence in the equilibrium diagrams may be somewhat different.

After a 20-min exposure at 900 $^{\circ}\text{C}$, cooling was performed at a constant rate of 2 $^{\circ}\text{C}/\text{min}$ down to $T \approx 150 \text{ }^{\circ}\text{C}$, and then the temperature decreased nonlinearly owing to the natural cooling of the

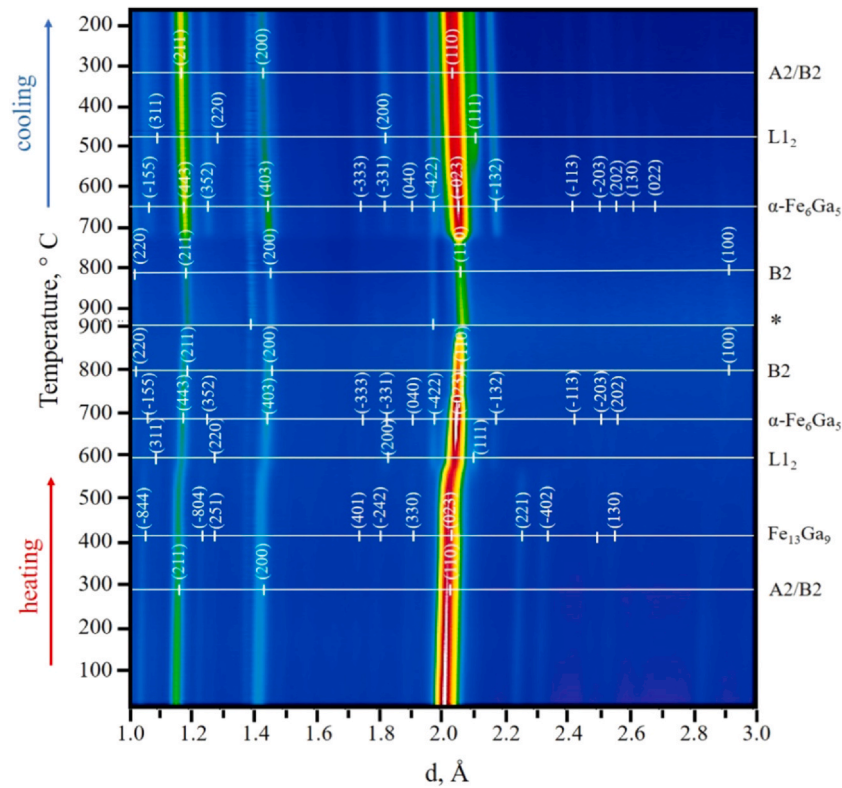


Fig. 2. 2D visualization of the neutron diffraction pattern evolution of the Fe-38.4Ga sample in the as-cast state measured upon slow heating up to 900 °C, annealing at this temperature for 20 min, and subsequent cooling down in the real-time mode. The temperature (and time) axis goes from bottom to top. Heating and cooling were performed with a rate close to 2 °C/min. The dashes indicate the peaks' positions from the phases indicated on the right. The symbol (*) denotes the peaks from the screens of the furnace in which the sample was located.

furnace. Phase transformations during cooling proceeded according to a scenario that significantly differed from the nonequilibrium phase diagram of Fe-Ga [8]. In particular, the transition from the single-phase B2 region to the two-phase B2 + α -Fe₆Ga₅ occurs at $T \approx 730$ °C. The release of the L₁₂ phase begins at $T \approx 570$ °C.

Upon cooling, the B2 phase does not disappear immediately upon reaching a temperature of 625 °C, which corresponds to the B2 + α -Fe₆Ga₅ → D0₁₉ transition according to the Fe-Ga phase diagram [8]. As shown below, the A2/B2 phase is present in the material until complete cooling, and it is detected at the beginning of the second heating-cooling cycle. It is known that bcc-based phases can be observed at low temperatures in Fe-Ga nonequilibrium alloys with the gallium content of 28.6–44.4 at%. Thus the paper [14] presents the phase analysis of alloys with 28.9, 32.9, and 38.4 at% Ga quenched from the melt and then annealed at 300–575 °C for 300 h. It was shown that the heat treatment time is insufficient for the transition of the alloys to the equilibrium state, and the bcc phase was present in all the studied states. Nevertheless, its volume fraction regularly decreased with an increase in the annealing temperature. Thus, we can argue that after the first heating-cooling cycle, the phase composition of the Fe-38.4Ga alloy corresponds to the state L₁₂ + α -Fe₆Ga₅ + A2/B2.

The *in situ* NDPs measured under the second heating-cooling cycle are presented in Fig. 6 and typical diffraction patterns measured at heating are shown in Fig. 7. The intensities of the peaks corresponding to the L₁₂ phase increase and the intensities of the peaks corresponding to the A2/B2 phase decrease upon heating in a temperature range of 460–600 °C. The intensity of the peaks of the α -Fe₆Ga₅ phase virtually does not change. The peaks corresponding

to the A2/B2 phase almost completely disappear upon reaching $T \approx 610$ °C. Thus, the transition of the alloy to the equilibrium L₁₂ + α -Fe₆Ga₅ state occurred, and an increase in the volume fraction of L₁₂ occurred completely due to a decrease of the nonequilibrium A2/B2 phase fraction.

Further, as the temperature rises above 600 °C, the formation of the B2 phase begins. A complete transition to the two-phase α -Fe₆Ga₅ + B2 state occurs after the disappearance of L₁₂ at $T \approx 650$ °C. The single-phase state B2 is reached at $T \approx 740$ °C, which is slightly higher than in the case of the first heating. During the second cooling, the precipitation of monoclinic α -Fe₆Ga₅ occurs at $T \approx 750$ °C and the diffraction peaks corresponding to L₁₂ appear at $T \approx 620$ °C. These temperatures are slightly (20–50 °C) higher than those of similar phase transitions in the first heating-cooling cycle.

The neutron diffraction pattern (Fig. 8) measured after two heating-cooling cycles shows L₁₂ and α -Fe₆Ga₅ as the main phases; however, the bcc-based phase is also seen. Obviously, the cooling rate (2 °C/min) does not provide a complete transition of the alloy to the equilibrium L₁₂ + α -Fe₆Ga₅ state. Weak peaks with $d = 2.28$, 2.46, and 3.35 Å are also found. They could not be assigned to any phase known for the Fe-Ga system.

3.2. Calorimetry and dilatometry

The as-cast Fe-38.4Ga alloy shows an exothermic reaction with a peak at 575 °C at heat flow curves at heating, which can be assigned to the appearance of the L₁₂ and α -Fe₆Ga₅ phases (Fig. 9). The transitions match the Fe-Ga diagram [15]. The change in the slope of the DSC curve at 680 °C recorded during heating (Fig. 9, Table 1)

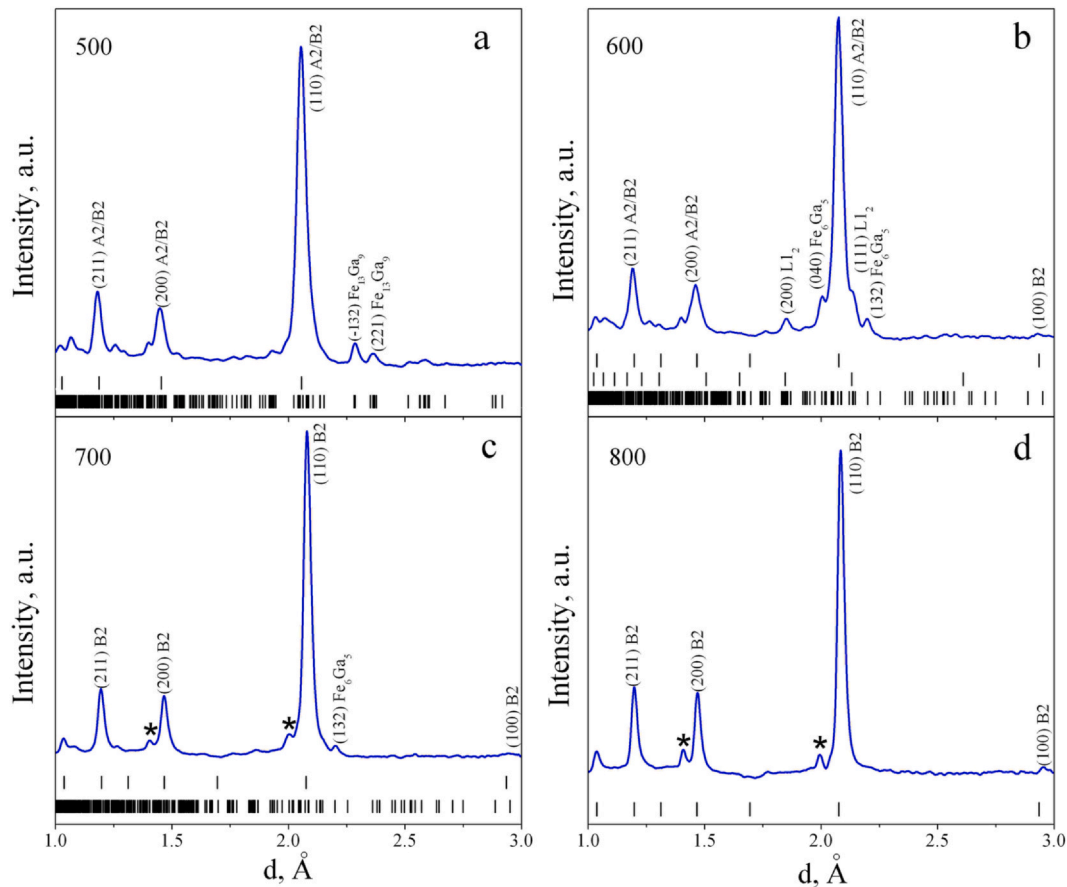


Fig. 3. ND patterns measured upon first heating for several characteristic temperatures. The vertical bars indicate the peak positions of the presented phases (from top to bottom): a – A2, $Fe_{13}Ga_9$; b – A2/B2, $L1_2$, $\alpha-Fe_6Ga_5$; c – B2, $\alpha-Fe_6Ga_5$; d – B2. The symbol (*) denotes the peaks (Al) from the screens of the furnace in which the sample was located.

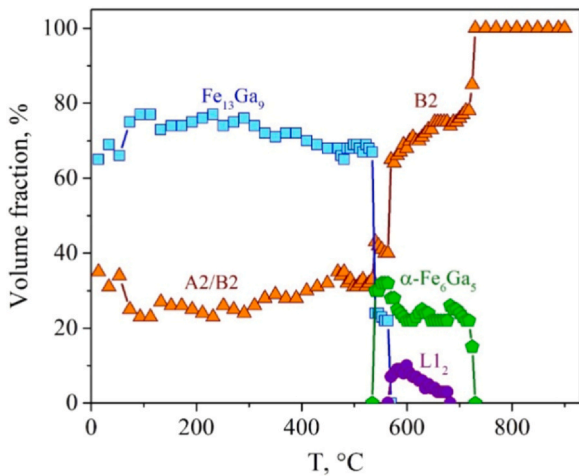


Fig. 4. Evolution of the phase composition of the Fe-38.4Ga alloy in the as-cast state upon heating to 900 °C.

corresponds to the disappearance of $L1_2$ and an increase in the volume fraction of the B2 phase (Fig. 4). The peak corresponding to the $\alpha-Fe_6Ga_5 + B2 \rightarrow B2$ transition is observed upon reaching 745 °C. Two peaks (Fig. 9, Table 2) that correspond to the transitions first from the B2 region to $\alpha-Fe_6Ga_5 + B2$ and then to $\alpha-Fe_6Ga_5 + L1_2 + A2/B2$ are observed upon cooling. It can be noted that the temperature of the $B2 \rightarrow B2 + \alpha-Fe_6Ga_5$ transition is significantly lower than that of

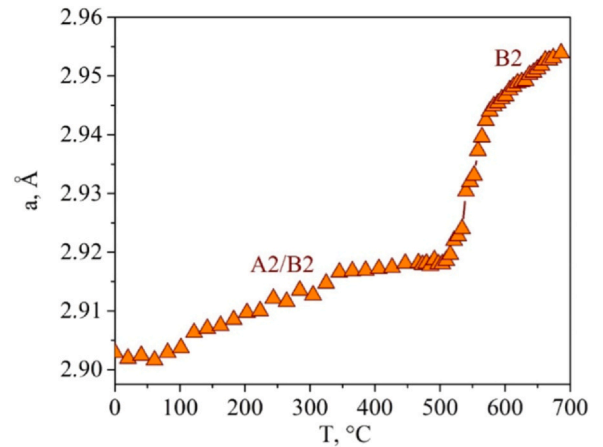


Fig. 5. Temperature dependence of the lattice parameter of the bcc based phases.

observed in the ND experiment. This is probably due to the differences in the experimental conditions, namely, in the rate of the temperature change. The temperature of the phase transformation $B2 + \alpha-Fe_6Ga_5 \rightarrow L1_2 + \alpha-Fe_6Ga_5 + A2/B2$ obtained both in ND and DSC analyses coincides quite well.

The dependencies of the linear expansion and its rate on the instant temperature for Fe-38.4Ga are shown in Fig. 10. The decrease in the slope of the linear expansion dependency noted at a

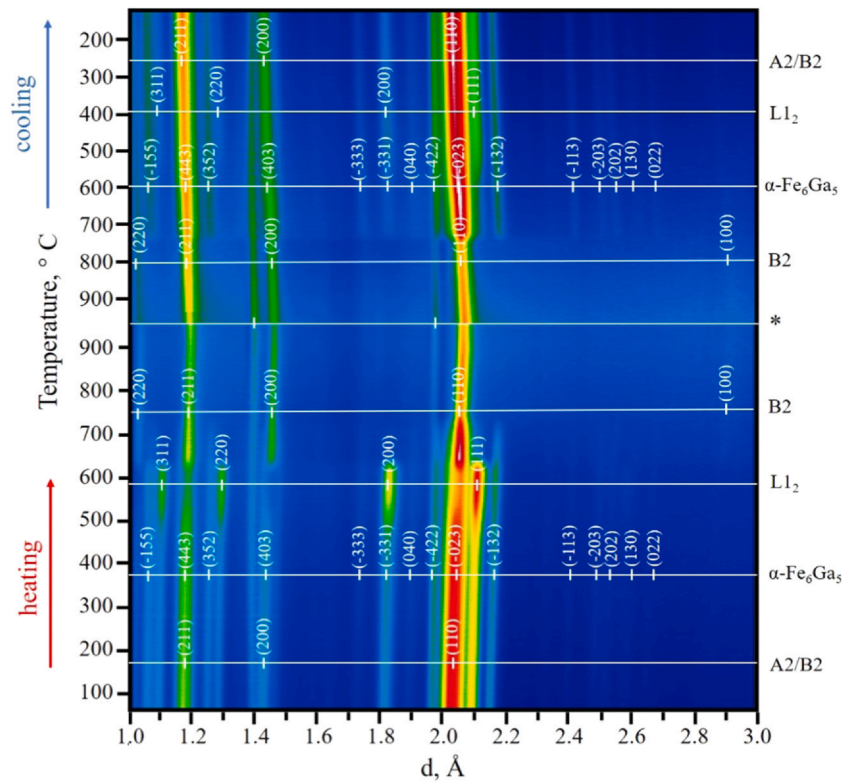


Fig. 6. 2D visualization of the neutron diffraction pattern evolution of the Fe-38.4Ga sample during the second heating-cooling cycle. The patterns were measured upon slow heating up to 900 °C, annealing at this temperature in 40 min, and subsequent cooling down in the real-time mode. The temperature (and time) axis goes from bottom to top. The dashes indicate the positions of the peaks from the phases indicated on the right. The symbol (*) denotes the peaks from the screens of the furnace in which the sample was located.

temperature of 585 °C can be explained by the same transition from the metastable structure with the A2/B2 + Fe₁₃Ga₉ to L₁₂ + α-Fe₆Ga₅ + A2/B2 phases. Here, we would also like to remind of a transient internal friction peak at about 580 °C reported in Ref. [12]. The second change in the slope that can be noted in the rate dependency (on the derivative curve) can correspond to the transition α-Fe₆Ga₅ + B2 to the B2 phase. It is in agreement with the neutron diffraction results.

The values of the phase transitions temperatures that occurred during single heating and subsequent cooling and determined by the ND, TDIF, DT, and DSC methods are summarized in Tables 1 and 2. A good correlation between the obtained values can be recognized.

4. Discussion

In [15], it was shown that the region of existence of the B2/B2' phase significantly expands to the region of low temperatures upon rapid cooling of alloys with a gallium concentration above 30 at%. B2', as well as B2, has a crystal structure based on a bcc lattice, and this separation was first adopted in Ref. [16]. In this paper, we make no distinction between B2 and B2' and then use only B2 designation. Depending on the preparation method, the phase composition in alloys with a gallium concentration from 28.4 to 40 at% according to Ref. [15] can be represented by a mixture of several phases from the following list: B2', M, L₁₂, α-Fe₆Ga₅, β-Fe₆Ga₅. The first two phases on this list are metastable. At the same time, in the powders of the alloy with a gallium concentration of 30.5–39.5 at% Ga upon quenching from 900 °C, only the B2 phase was revealed by X-ray diffraction analysis, and in the region of 39.5–45.0 at% Ga, a mixture of the B2, M, and β-

Fe₆Ga₅ phases was detected [15]. The metastable M phase corresponds to the Fe₁₃Ga₉ phase recently deciphered in Ref. [5]. Thus the phase composition A2/B2 + Fe₁₃Ga₉ of the studied Fe-38.4Ga alloy in the as-cast state, on the one hand, fully corresponds to the set of phases that may arise, but, on the other hand, does not correspond to the quenched states near 39.5 at% Ga concentration. Possibly, one can distinguish the concentration range with a nonequilibrium phase composition B2 + M, obtained as a result of rapid cooling from the melt or high temperatures region.

Upon heating at a rate of 2 °C/min, the Fe₁₃Ga₉ phase indicated in the diagram [7] as the metastable M-phase completely disappears at about 570 °C. This temperature coincides with the temperature of the peritectoid reaction B2 + α-Fe₆Ga₅ → M (570 °C) [15]. At the same time, it was indicated in [5] that the transition from Fe₁₃Ga₉ + A2/B2 to L₁₂ + α-Fe₆Ga₅ in the Fe-38.4Ga alloy was observed already at 500 °C.

An abrupt increase in the lattice parameter of the phase based on the bcc lattice is observed in the temperature range in which the disappearance of Fe₁₃Ga₉ is observed (Fig. 5). It can be assumed that it is due to an increase in the gallium concentration in this phase. Indeed, the volume fraction of the Fe₁₃Ga₉ phase in the initial state is ~70%. Fe₁₃Ga₉ has a sufficiently high gallium concentration according to the stoichiometric composition (Table 3), which is calculated based on the formula unit of the phase. This means that when Fe₁₃Ga₉ disappeared, a large amount of gallium was released. Part of gallium was involved in the formation of α-Fe₆Ga₅, the maximum volume fraction of which is ~30%, according to the estimates made by the Rietveld method (Fig. 4). L₁₂ is capable of dissolving up to 29.2 at% Ga [8], but its volume fraction in the alloy is also low.

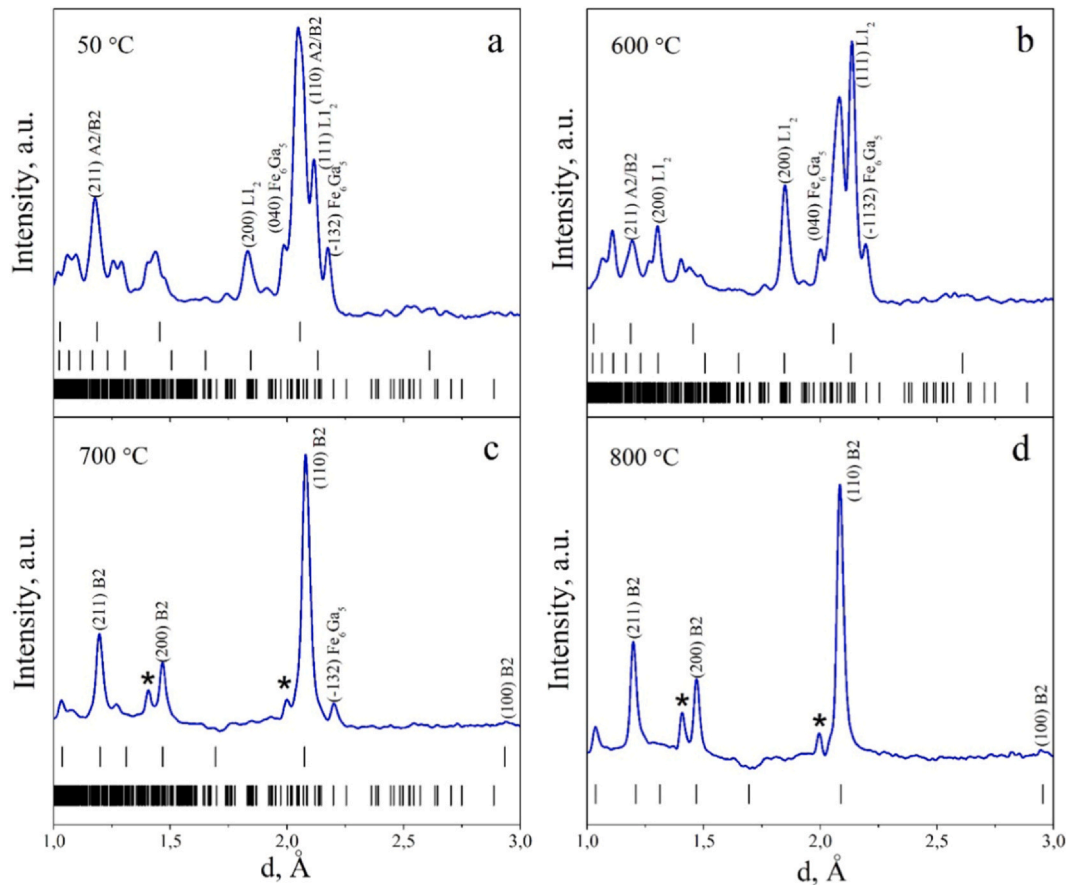


Fig. 7. ND patterns measured upon second heating for several characteristic temperatures. The vertical bars indicate the peak positions of the presented phases (from top to bottom): a – A2, L1₂, α-Fe₆Ga₅; b – B2, L1₂, α-Fe₆Ga₅; c – B2, α-Fe₆Ga₅; d – B2. The symbol (*) denotes the peaks (Al) from the screens of the furnace in which the sample was located.

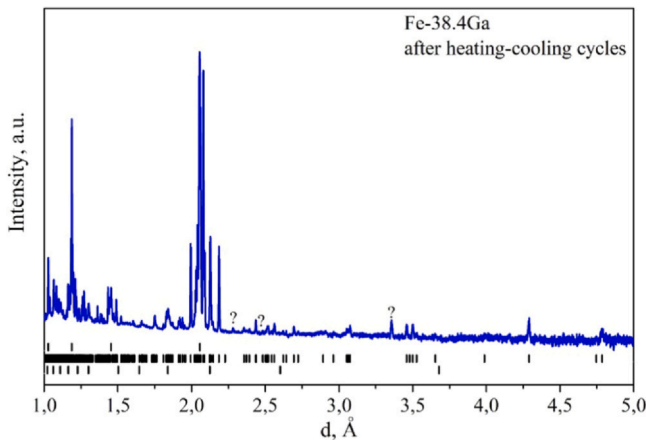


Fig. 8. ND pattern of the Fe-38.4Ga sample after two heating-cooling cycles. The vertical bars indicate the peak positions (from top to bottom) of: A2 (1), α-Fe₆Ga₅ (2), L1₂ (3). Several non-indexed lines are marked by ?.

Note that, according to the work of Okamoto [8], at temperatures below 900 °C, three phase transitions should be observed upon cooling for the Fe-38.4Ga alloy:

- (1) B2 → B2 + α-Fe₆Ga₅ (730 °C),
- (2) B2 → D0₁₉ + α-Fe₆Ga₅ (625 °C),
- (3) D0₁₉ + α-Fe₆Ga₅ → L1₂ (619 °C).

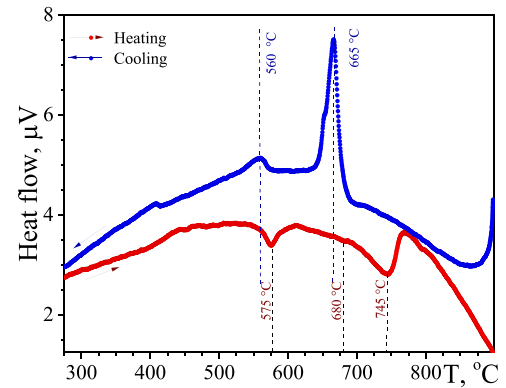


Fig. 9. Heat flow dependencies on the temperature for the as cast Fe-38.4Ga alloy.

So, there is a disagreement between the state diagrams of Okamoto and Gödeke-Köster. As shown in this work, a two-phase L1₂ + α-Fe₆Ga₅ state is formed upon transition to an equilibrium state in the temperature range below 619 °C, rather than L1₂, as follows from [8]. But this phase composition is in agreement with the diagram given in [16].

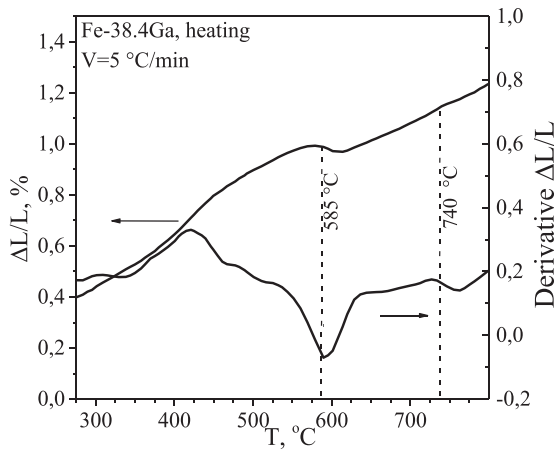
In all the studied states, the α-Fe₆Ga₅ phase was found with crystal lattice parameters (Table 4) significantly different from those given in Ref. [17]. A search in the Materials Project database [18], which presents the results of numerical modeling of various materials by the DFT method, showed that the parameter *c* and angle β

Table 1
Temperatures of the phase transitions during first heating according to different techniques.

	ND	TDIF	DT	DSC
Heating rate, °C/min	2	2	5	10
A2/B2 + Fe ₁₃ Ga ₉ → L ₁₂ + α-Fe ₆ Ga ₅ + B2				
T, °C	570	582	585	575
L ₁₂ + α-Fe ₆ Ga ₅ + B2 → α-Fe ₆ Ga ₅ + B2				
T, °C	660	–	–	680
α-Fe ₆ Ga ₅ + B2 → B2				
T, °C	720	–	740	745

Table 2
Temperatures of the phase transitions during first cooling according to different techniques.

	ND	TDIF	DSC
Heating rate, °C/min	2	2	10
B2 → B2 + α-Fe ₆ Ga ₅			
T, °C	725	–	665
B2 + α-Fe ₆ Ga ₅ → L ₁₂ + α-Fe ₆ Ga ₅ + A2/B2			
T, °C	570	550	560

**Fig. 10.** Thermal expansion dependencies on temperature for the as cast Fe-38.4Ga alloy.**Table 3**
Composition of the phases in the Fe-38.4Ga alloy.

Phase	Fe, at%		Ga, at%	
	Stoichiometry	Phase diagram Fe-Ga [8]	Stoichiometry	Phase diagram Fe-Ga [8]
Fe ₁₃ Ga ₉	59.1	–	40.9	–
α-Fe ₆ Ga ₅	54.5	55.5–54.5	45.5	44.5–45.5
L ₁₂ (Fe ₃ Ga)	75	71.8–73.8	25	26.2–29.2
B2(FeGa)	50	52.5–68.5	50	31.5–47.5

Table 4
Lattice constant of α-Fe₆Ga₅ phase.

Source	a, Å	b, Å	c, Å	β, °
[17]	10.058 ± 0.005	7.946 ± 0.005	7.747 ± 0.005	109.33 ± 0.16
[19]	10.040	7.918	7.689	108.38
Our data	10.081 ± 0.002	7.975 ± 0.002	7.699 ± 0.002	108.34 ± 0.10

obtained in the experiment are in good agreement with the theoretically calculated values. Still, there are significant discrepancies for the parameters *a* and *b* (Table 2) [19]. Such discrepancies in the calculated and experimental data can be associated with both the inaccuracy of the theoretical methods used and the presence of the residual A2/B2 phase. Nevertheless, the mean absolute error (MAE) for the distances between the nearest neighbors Fe-Fe, Fe-Ga, and Ga-Ga does not exceed 0.02 Å. It is an excellent result for the DFT analysis [20].

According to the phase diagrams [8,16], the hcp-based D0₁₉ could form during cooling of the Fe-38.4 Ga alloy from the high-temperature region. But it was impossible to record that phase in the diffraction patterns neither in the first nor in the second heating-cooling cycles. A similar situation was observed in Refs. [21,22]. It was shown for the Fe-27Ga alloy that at high cooling rates, the following sequence of phase transitions B2 → A2 → A1 → L₁₂ was realized. The A2 → A1 transition is realized by a bcc to fcc lattice transition according to the Bain scheme and is described in detail in the works [23,24]. Therefore, it is logical to assume that in the Fe-38.4 Ga alloy, the transformation of the nonequilibrium A2/B2 phase into the equilibrium L₁₂ phase follows the same scheme in the temperature range below 606 °C. This is especially noticeable in the second heating cycle when an increase in the volume fraction L₁₂ was carried out completely due to a decrease in the fraction of the A2 phase during the transition of the alloy to the equilibrium state.

A few more interesting points should be noted. The second cycle is distinguished by a higher temperature value of the forward α-Fe₆Ga₅ + B2 → B2 and reverse B2 → α-Fe₆Ga₅ + B2 phase transitions compared to the first cycle. In both cycles, the α-Fe₆Ga₅ + B2 → B2 phase transition upon heating occurred at a temperature somewhat lower than the reverse transition upon cooling, although the

opposite situation should have been observed. The only difference between two heating cycles in the high-temperature region is that during the first heating cycle, the formation of the ordered B2 phase was essentially carried out from a nonequilibrium state, which is characterized by the presence of the A2/B2 phase. In the second cycle, B2 already formed from the $L1_2 + \alpha\text{-Fe}_6\text{Ga}_5$ state. It can be assumed that due to the low diffusion mobility of atoms in alloys of the Fe-Ga system [4,25], the temperatures of phase transformations occurring both upon heating and cooling depend on what preliminary state was formed in the material. Namely, this depends on whether the distribution of elements in individual phases corresponds to an equilibrium state.

5. Conclusion

Our research into the phase composition evolution in the Fe-38.4Ga alloy during two heating-cooling cycles showed the following:

1. The first phase transformation upon heating at a rate of 2 °C/min of the Fe-38.4Ga alloy in the nonequilibrium $\text{Fe}_{13}\text{Ga}_9 + \text{A2/B2}$ state is observed at ~570 °C. It represents the complete disappearance of $\text{Fe}_{13}\text{Ga}_9$ and the appearance of $\alpha\text{-Fe}_6\text{Ga}_5$ and $L1_2$, while the A2/B2 phase retains its existence in the alloy. This temperature fully coincides with the temperature of the peritectoid reaction given earlier for the metastable M-phase in Ref. [16].
2. The further order of phase transformations during heating and cooling, both in the first and the second cycles, corresponds to the phase diagram of Fe-Ga, but there are differences in the temperatures at which they occur. In particular, in two cycles, the transition temperatures $L1_2 + \alpha\text{-Fe}_6\text{Ga}_5 \rightarrow \text{B2}$ change upon heating and $\text{B2} \rightarrow L1_2 + \alpha\text{-Fe}_6\text{Ga}_5$ upon cooling. These differences may be associated with a low rate of diffusion processes in the Fe-Ga system. In fact, the time of existence at the temperature of the phase transformation is insufficient to achieve an equilibrium state. Probably, the residual nonequilibrium A2/B2 phase remains at low temperatures for the same reason.
3. The crystal lattice parameters of the $\alpha\text{-Fe}_6\text{Ga}_5$ phase precipitated in all the studied states differ from the experimental data given in Malaman's work [17] but are in good agreement with the numerically calculated values given in the database [19].

CRedit authorship contribution statement

T.N. Vershinina: Investigation, Writing – original draft. **I.A. Bobrikov:** Investigation, Writing – review & editing. **S.V. Sumnikov:** Investigation. **A.M. Balagurov:** Supervision, Conceptualization, Data analysis, Writing – review & editing. **A.K. Mohamed:** Investigation. **I.S. Golovin:** Conceptualization, Writing – review & editing, Funding acquisition.

Declaration of Competing Interest

The authors declare that they have no known competing financial interests or personal relationships that could have appeared to influence the work reported in this paper.

Acknowledgments

The neutron diffraction data were obtained using the IBR-2 (JINR) neutron source. The authors are grateful to V.G. Simkin for assistance with the neutron diffraction experiment and Dr. E.M. Bazanova for critical reading the manuscript. This study was supported by Russian Science Foundation project 19-72-20080.

References

- [1] E.M. Summers, T.A. Lograsso, M. Wun-Fogle, Magnetostriction of binary and ternary Fe-Ga alloys, *J. Mater. Sci.* 42 (2007) 9582–9594, <https://doi.org/10.1007/s10853-007-2096-6>
- [2] Q. Xing, Y. Du, R.J. McQueeney, T.A. Lograsso, Structural investigations of Fe-Ga alloys: phase relations and magnetostrictive behavior, *Acta Mater.* 56 (2008) 4536–4546, <https://doi.org/10.1016/j.actamat.2008.05.011>
- [3] J. Atulasimha, A.B. Flatau, A review of magnetostrictive iron-gallium alloys, *Smart Mater. Struct.* 20 (2011) 043001, <https://doi.org/10.1088/0964-1726/20/4/043001> (15pp).
- [4] I.S. Golovin, V.V. Palacheva, A.K. Mokhamed, A.M. Balagurov, Structure and properties of Fe-Ga alloys as promising materials for electronics, *Phys. Met. Metallogr.* 121 (2020) 851–893, <https://doi.org/10.1134/S0031918X20090057>
- [5] A. Leineweber, H. Becker, A.O. Boev, I.A. Bobrikov, A.M. Balagurov, I.S. Golovin, $\text{Fe}_{13}\text{Ga}_9$ intermetallic in bcc-base Fe-Ga alloy, *Intermetallics* 131 (2021) 107059, <https://doi.org/10.1016/j.intermet.2020.107059>
- [6] T.N. Vershinina, I.A. Bobrikov, S.V. Sumnikov, A.O. Boev, A.M. Balagurov, A.K. Mohamed, I.S. Golovin, Crystal structure and phase composition evolution during heat treatment of Fe-45Ga alloy, *Intermetallics* 131 (1–5) (2021) 107110, <https://doi.org/10.1016/j.intermet.2021.107110>
- [7] W. Koster, T. Godecke, Über den Aufbau des Systems Eisen-Gallium zwischen 10 und 50 at% Ga und dessen Abhängigkeit von der Wärmebehandlung. II. Das Gleichgewichtsdiagramm, *Z. Metallkd.* 68 (1977) 661–666.
- [8] H. Okamoto, The Fe-Ga (iron-gallium) system, *Bull. Alloy Phase Diagr.* 11 (1990) 576–581, <https://doi.org/10.1007/BF02841721>
- [9] A.M. Balagurov, Scientific reviews: high-resolution Fourier diffraction at the IBR-2 reactor, *Neutron News* 16 (3) (2005) 8–12, <https://doi.org/10.1080/10446830500454346>
- [10] J. Rodriguez-Carvajal, Recent advances in magnetic structure determination by neutron powder diffraction, *Physica B: Condensed Matter* 192 (1993) 55–69, [https://doi.org/10.1016/0921-4526\(93\)90108-1](https://doi.org/10.1016/0921-4526(93)90108-1)
- [11] L. Lutterotti, S. Matthies, H. Wenk, MAUD: a friendly Java program for material analysis using diffraction, *IUCr: Newsl. CPD* 21 (1999) 14–15.
- [12] I.S. Golovin, A.K. Mohamed, V.V. Palacheva, E.N. Zanaeva, J. Cifre, N.Yu Samoylova, A.M. Balagurov, Mechanical spectroscopy of phase transitions in Fe-(23–38)Ga-RE alloys, *J. Alloy. Compd.* 874 (2021) 159882, <https://doi.org/10.1016/j.jallcom.2021.159882>
- [13] M.V. Matyunina, M.A. Zagrebin, V.V. Sokolovskiy, O.O. Pavlukhina, V.D. Buchelnikov, A.M. Balagurov, I.S. Golovin, Phase diagram of magnetostrictive Fe-Ga alloys: insights from theory and experiment, *Phase Transit.* 92 (2) (2018) 101–116, <https://doi.org/10.1080/01411594.2018.1556268>
- [14] A.K. Mohamed, V.V. Palacheva, V.V. Cheverikin, E.N. Zanaeva, W.C. Cheng, V. Kulitckii, S. Divinski, G. Wilde, I.S. Golovin, The Fe-Ga phase diagram: revisited, *J. Alloy. Compd.* 846 (2020) 156486, <https://doi.org/10.1016/j.jallcom.2020.156486>
- [15] W. Koster, T. Godecke, Über den Aufbau des Systems Eisen-Gallium zwischen 10 und 50 at% Ga und dessen Abhängigkeit von der Wärmebehandlung. III. Ein Unterkühlungsdiagramm und Diagramme für die Vorgänge beim Anlassen ofgekühlter und abgeschreckter Legierungen, *Z. Metallkd.* 68 (1977) 758–764.
- [16] W. Koster, T. Godecke, Über den Aufbau des Systems Eisen-Gallium zwischen 10 und 50 at% Ga und dessen Abhängigkeit von der Wärmebehandlung. I. Das Diagramm der raumzentrierten Phasen, *Z. Metallkd.* 68 (1977) 582–589.
- [17] B. Malaman, M.J. Phillippe, B. Roques, A. Courtois, J. Protas, Structures cristallines des phases Fe_6Ge_5 et Fe_6Ga_5 , *Acta Cryst. B* 30 (1974) 2081–2087, <https://doi.org/10.1107/S056774087400652> (<https://materialsproject.org/>).
- [18] The Materials Project, Materials Data on Ga_5Fe_6 by Materials Project, United States: N. p., 2015. Web. (<https://doi.org/10.17188/1276000>).
- [19] K. Lejaeghere, V. Van Speybroeck, G. Van Oost, S. Cottenier, Error estimates for solid-state density-functional theory predictions: an overview by means of the ground-state elemental crystals, *Crit. Rev. Solid State Mater. Sci.* 39 (1) (2014) 1–24, <https://doi.org/10.1080/10408436.2013.772503>
- [20] I.S. Golovin, A.K. Mohamed, I.A. Bobrikov, A.M. Balagurov, Time-temperature-transformation from metastable to equilibrium structure in Fe-Ga, *Mater. Lett.* 263 (4p) (2020) 127257, <https://doi.org/10.1016/j.matlet.2019.127257>
- [21] I.S. Golovin, A.M. Balagurov, I.A. Bobrikov, S.V. Sumnikov, A.K. Mohamed, Cooling rate as a tool of tailoring structure of Fe-(9–33%) Ga alloys, *Intermetallics* 114 (2019) 106610, <https://doi.org/10.1016/j.intermet.2019.106610>
- [22] A.G. Khachatryan, D. Viehland, Structurally heterogeneous model of extrinsic magnetostriction for FeGa and similar. Magnetic alloys: part I. Decomposition and confined displacive transformation, *Metall. Mater. Trans. A* 38 (2007) 2308–2316, <https://doi.org/10.1007/s11661-007-9253-z>
- [23] A.M. Balagurov, N.Yu Samoylova, I.A. Bobrikov, S.V. Sumnikov, I.S. Golovin, The first- and second-order isothermal phase transitions in Fe_3Ga -type compounds, *Acta Cryst. B* 75 (6) (2019) 1024–1033, <https://doi.org/10.1107/S2052520619013106>
- [24] G.M. Muralikrishna, B. Tas, N. Esakiraja, V. Esin, K.C. Hari Kumar, I.S. Golovin, I.V. Belova, G.E. Murch, A. Paul, S.V. Divinski, Composition dependence of tracer diffusion coefficients in Fe-Ga alloys: a case study by a tracer-diffusion couple method, *Acta Mater.* 203 (2021) 116446, <https://doi.org/10.1016/j.actamat.2020.10.065>